PERGAMON

International Journal of Multiphase Flow 25 (1999) 459–476

International Journal of Multiphase Flow

Near wall structure in vertical air–water annular flows

P. Vassallo

Lockheed Martin Corporation, P.O. Box 1072, Schenectady, NY 12309, USA

Received 28 July 1997; received in revised form 18 August 1998

Abstract

Annular flow topology for three air–water conditions in a vertical duct is investigated through the use of a traversing double-sensor hot-film anemometry probe and differential pressure measurements. Near wall measurements of mean and fluctuating velocities, as well as local void fraction, are taken in the liquid film, with the highest turbulent fluctuations occurring for the flow condition with the largest pressure drop. A modified law-of-the-wall formulation for wall shear is presented which, using near wall values of mean velocity and kinetic energy, agrees reasonably well with the average stress obtained from direct pressure drop measurements. The linear profile using wall coordinates in the logarithmic layer is preserved in annular flow; however, the slope and intercept of the profile differ from the single-phase values for the annular flow condition which has a thicker, more turbulent, liquid film.

Keywords: Annular flow; Liquid film; Hot-film anemometry; Wall shear; Law-of-the-wall; Pressure drop; Turbulence; Void fraction

1. Introduction

As described by Hewitt and Whalley (1989), annular flow in a conduit consists of a high velocity gas core in the center of the conduit and a thin liquid film on the conduit walls. The interaction between gas core and liquid film produces a wavy structure at the gas–liquid interface which, in turn, affects the turbulent structure in the film. The frictional pressure drop, or wall shear, is ultimately related to the turbulent structure in the film. Quantitative near wall turbulence measurements in annular flow are therefore needed to help develop analytical models, and to qualify numerical codes, which are used to predict overall pressure drop.

As an example, law-of-the-wall modeling is used extensively in single-phase codes to relate the wall shear stress to the velocity field away from the wall as an alternative to prohibitively

0301-9322/99/$ - see front matter. Published by Elsevier Science Ltd.
PII: S0301-9322(98)00052-4

small grids. Similar formulations are used in many two-phase codes, primarily because the effect of the second phase on the law-of-the-wall is not well understood. Thus, there is a need for near wall turbulence data in order to better understand the effect, particularly for the case of annular flow.

Most of the previous studies in vertical annular flow have been focused on liquid film thickness [e.g. Bellinghausen and Renz (1992)], wave structure [e.g. Asali and Hanratty (1993)] and pressure drop measurements [e.g. Govan et al. (1989)]; no data appears to be available which provides information on the turbulent near wall structure in the film. In horizontal stratified flow, Lorencez et al. (1997) did measure the turbulence level in the gas and liquid phases and found that the turbulence level in the film increased as the interfacial shear increased. Several papers are also available which provide turbulence data in bubbly flow conditions, among them Velidandla et al. (1996) and Marie et al. (1997). In these papers, near wall velocities were measured and it was determined that the linear log-law was preserved near the wall, but with different values of the coefficients. If, as Hewitt et al. (1990) observed, bubbles are continuously being generated and released by the rolling action of the waves in annular flow, a connection might be made between the near wall structure in both the bubbly and annular regimes. This paper attempts to examine the relationship between the turbulent structure in the liquid film and the wall shear stress in the context of the classical law-of-the-wall formulation.

2. Experimental description

2.1. Test section and related instrumentation

The air–water flow loop consists of a transparent test section, pump, air–water separator, and several rotameters and pressure gauges for the measurement of air and water flow rates. A schematic of the test section is given in Fig. 1. The test section, made from cast acrylic components, is about 170 cm long, with a cross-sectional flow area of 6.35×0.635 cm (hydraulic diameter, $D_h = 1.15$ cm). The test section has eight removable windows on the transverse walls into which instrumentation may be mounted.

Fig. 1 shows the locations of the quick-closing valves and the pressure taps. The quick-closing valves were used to obtain the average static void fraction. The pressure taps (0.25 mm diameter) were installed in two of the test section faces in order to measure the frictional pressure drop. The pressure drop was measured using calibrated ($\pm 0.5\%$) Rosemont transducers with an estimated total uncertainty of $\pm 4\%$, based on the observed scatter in repeated measurements.

2.2. Hot-film anemometry (HFA)

A quartz coated TSI double-sensor hot-film probe (model 1244-10AW) was mounted in a traversing mechanism to allow for motion across the narrow test section dimension. The probe was located near the exit of the test section, at an axial position of $Z = 152.2$ cm ($Z/D_h = 132$) and a transverse position of $X = 3.2$ cm. Each of the probe's two cylindrical sensors had an

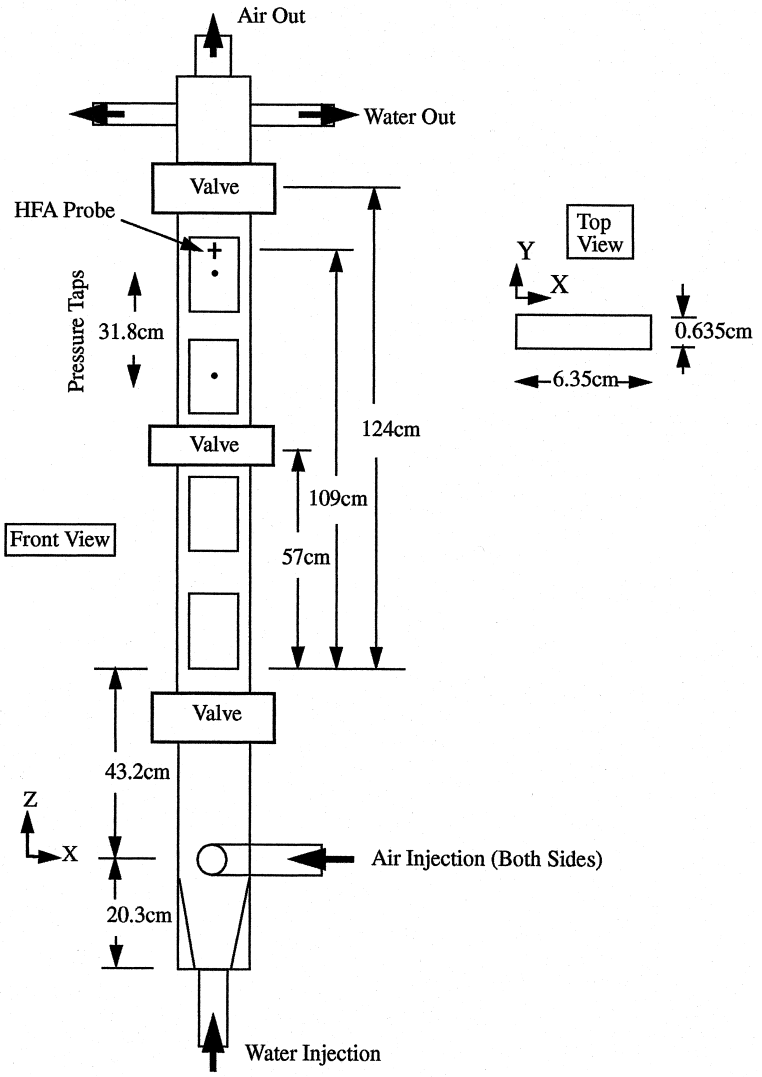

Fig. 1. Test section schematic.

active length of 0.178 mm, and a diameter of 0.038 mm; the spacing between sensors was 1 mm.

The HFA probe was designed to minimize perturbation effects on the flow. As seen in Fig. 2, the probe sides were extended downward 267 film diameters to isolate the sensitive element from the traversing rod. In addition, the sensitive element was centered 4 film lengths from the probe sides via film supports to reduce flow splashing around the sides. Generally, then, the HFA technique is considered reliable if the liquid phase encompasses the sensitive element. This is readily accomplished near the wall as the liquid film thickness for the annular flows studied here is about 16 times the film diameter. As the probe is moved closer to the liquid film interface, uncertainties will increase, as discussed further in Section 3.4.

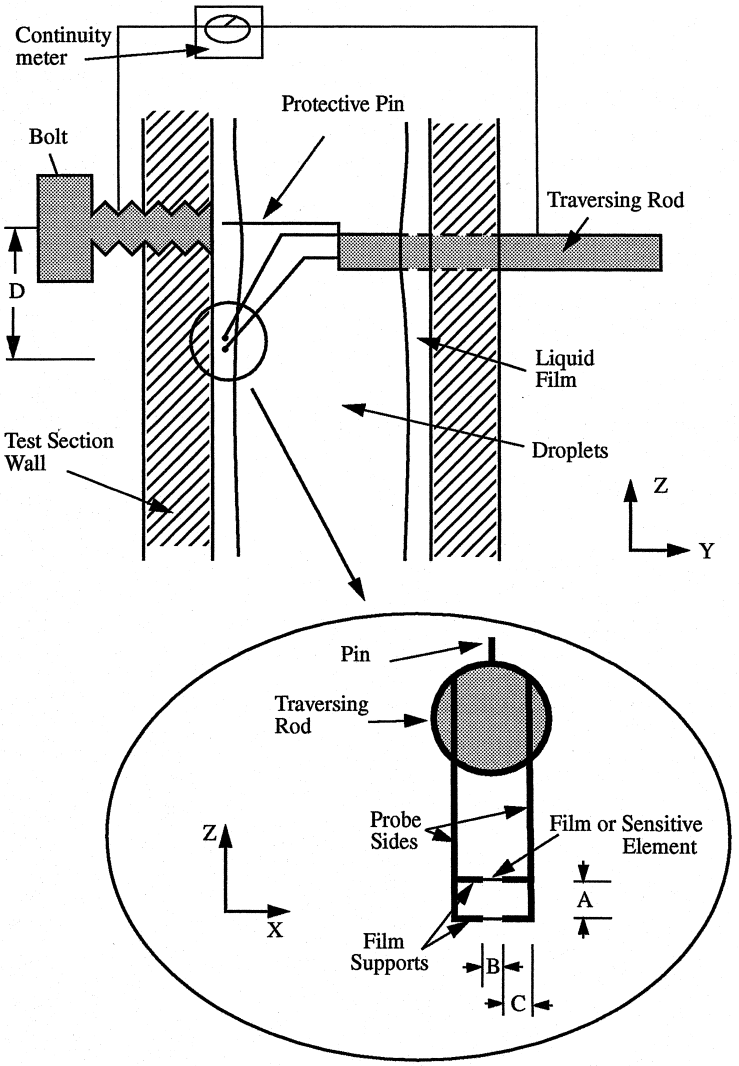

Fig. 2. Sketch of HFA probe in test section; (A) = 1 mm, (B) = 0.18 mm, (C) = 0.72 mm, (D) = 10 mm. Film: 38 μm diameter. Film supports: 152 μm diameter.

The HFA probe was equipped with a pin which extended 0.076 mm past the outermost sensor. This pin protected the sensor from damage as the probe was moved close to the far wall. A 6.35 mm diameter bolt was machined flat and screwed into the far wall to serve as a detection point for the probe. When the pin touched the bolt, a circuit was established and defined the first measurement location at a position 0.076 mm from the wall. The probe was then retracted across the test section as measurements were taken. The uncertainty in HFA positioning was estimated to be $\pm$0.025 mm.

Local void fraction, liquid velocity and interfacial velocity were obtained with the HFA probe. For void fraction and liquid velocity, only the upstream sensor in the double wire probe

Table 1
Comparison of measurements taken in sequence (each data record = 6.4 s)

Y/t (t = 6.35 mm)	j_l (m/s)	j_g (m/s)	U (m/s)	u' (m/s)	α
0.012	1.3	12.8	2.38	0.96	0.01
0.012	1.3	12.8	2.37	0.99	0.01
0.068	1.3	12.8	3.09	0.80	0.48
0.068	1.3	12.8	3.12	0.84	0.51
0.012	0.65	20.4	2.51	0.79	0.03
0.012	0.65	20.4	2.63	0.80	0.02
0.068	0.65	20.4	3.5	0.68	0.66
0.068	0.65	20.4	3.58	0.72	0.68

was used; for interfacial velocity, both sensors were used. The overheat ratio (the ratio of operating resistance to the resistance at ambient temperature) was about 1.1. A total of 6.4 s of data were taken at each point at a sampling rate of 10 kHz; repeated measurements showed reasonable convergence of the mean velocity, U, the fluctuating velocity, u', and void fraction, α, as shown in Table 1 for given values of liquid and gas superficial velocity. The water temperature was maintained at $32.2^{\circ}C \pm 0.2^{\circ}C$.

To obtain liquid velocity statistics (both mean and fluctuating quantities), the HFA probe was first calibrated in single-phase liquid flow using laser doppler velocimetry to measure velocity. A constant temperature was maintained at the hot-film; for a given operating resistance, the change in voltage corresponded to a change in velocity. During the early phase of this work, a slow downward drift in HFA voltage was observed at a constant liquid flow rate; apparently, due to small loop contaminants in the deionized water collecting on the probe and changing its heat transfer characteristics. To reduce contamination uncertainties, the probe was run in the high velocity annular flow condition for about 30 min, and then quickly calibrated (in a period of about 5 min) over a range of liquid velocities, with the last calibration being a repeat of the first to ensure that significant drift was not occurring. The HFA measurements in the annular flow condition were then taken. Finally, the air was turned off, and the calibration measurements were repeated. This approach effectively eliminated any concerns about drift in the HFA probe voltage during data acquisition.

For determination of liquid velocity, the HFA voltage traces acquired in two-phase flow had to be processed to remove the vapor part of the signals. This was accomplished by using a program developed by Lee (1982) which employs both level and slope thresholding. When a vapor interface contacts the probe, the voltage level decreases abruptly. A slope threshold can be established so that when the voltage gradient exceeds the threshold value, the signal is taken as part of the vapor phase. Level thresholding is also employed to improve the accuracy of the method. The level threshold was obtained by visual examination of the voltage traces. The slope threshold was estimated from oscilloscope voltage traces and was about twice the value of the maximum slope observed in all liquid flow. The results were not very sensitive to this

selection; Table 2 shows calculated values of void fraction and fluctuating velocities for the same voltage trace as a function of slope and level threshold.

The validity of the void discrimination program was assessed in several ways. First, pre-generated signals using modified square waves were analyzed to confirm that the calculated void fractions agreed precisely with the known values. Next, for several low void fraction bubbly cases, the number of bubbles in the raw HFA voltage trace were manually counted and found to be in good agreement with the number of bubbles determined from the program. Finally, as will be seen later, the integrated average of cross sectional HFA void fraction agreed well with the average void fraction obtained with quick closing valves.

The velocity of the passing interfaces in the two-phase mixture was obtained by cross correlating the signals from each of the two HFA sensors using a signal analyzer. This resulted in a most probable time required for the interfaces to travel between the two sensors. The mean interfacial velocity was calculated by dividing the known sensor spacing (1 mm) by this time. The random uncertainty in velocity, based on repeated measurements, is estimated to be $\pm 5\%$.

Table 2
Effect of threshold parameters on calculated results[1]

j_l (m/s)	j_g (m/s)	Y/t (t = 6.35 mm)	Level (V)	Slope (V/ms)	α	U (m/s)	u' (m/s)
1.3	12.8	0.012	0.3	0.5	0.016	2.39	0.95
1.3	12.8	0.012	0.2	0.4	0.014	2.37	0.96
1.3	12.8	0.012	0.2	0.5	0.009	2.37	0.96
1.3	12.8	0.012	0.2	0.6	0.008	2.37	0.97
1.3	12.8	0.012	0.1	0.5	0.008	2.36	0.97
1.3	12.8	0.068	0.3	0.5	0.50	3.13	0.77
1.3	12.8	0.068	0.2	0.4	0.53	3.11	0.77
1.3	12.8	0.068	0.2	0.5	0.49	3.13	0.78
1.3	12.8	0.068	0.2	0.6	0.48	3.13	0.78
1.3	12.8	0.068	0.1	0.5	0.49	3.12	0.79
0.65	20.4	0.012	0.3	0.5	0.021	2.52	0.78
0.65	20.4	0.012	0.2	0.4	0.024	2.52	0.79
0.65	20.4	0.012	0.2	0.5	0.02	2.51	0.79
0.65	20.4	0.012	0.2	0.6	0.017	2.51	0.79
0.65	20.4	0.012	0.1	0.5	0.019	2.51	0.79
0.65	20.4	0.068	0.3	0.5	0.66	3.54	0.62
0.65	20.4	0.068	0.2	0.4	0.67	3.54	0.63
0.65	20.4	0.068	0.2	0.5	0.66	3.53	0.65
0.65	20.4	0.068	0.2	0.6	0.65	3.52	0.65
0.65	20.4	0.068	0.1	0.5	0.65	3.52	0.66

[1]The following threshold parameters were used in this work: level, 0.2 V; slope, 0.5 V/ms.

3. Results

3.1. Single-phase flow

Single-phase liquid measurements of mean and fluctuating velocities were taken across the test section thickness dimension to verify the HFA technique. The results are presented in terms of Y/t, where Y is the position along the narrow duct dimension and t is the duct thickness. The calibration curve used to determine velocity is shown in Fig. 3(a). The points on

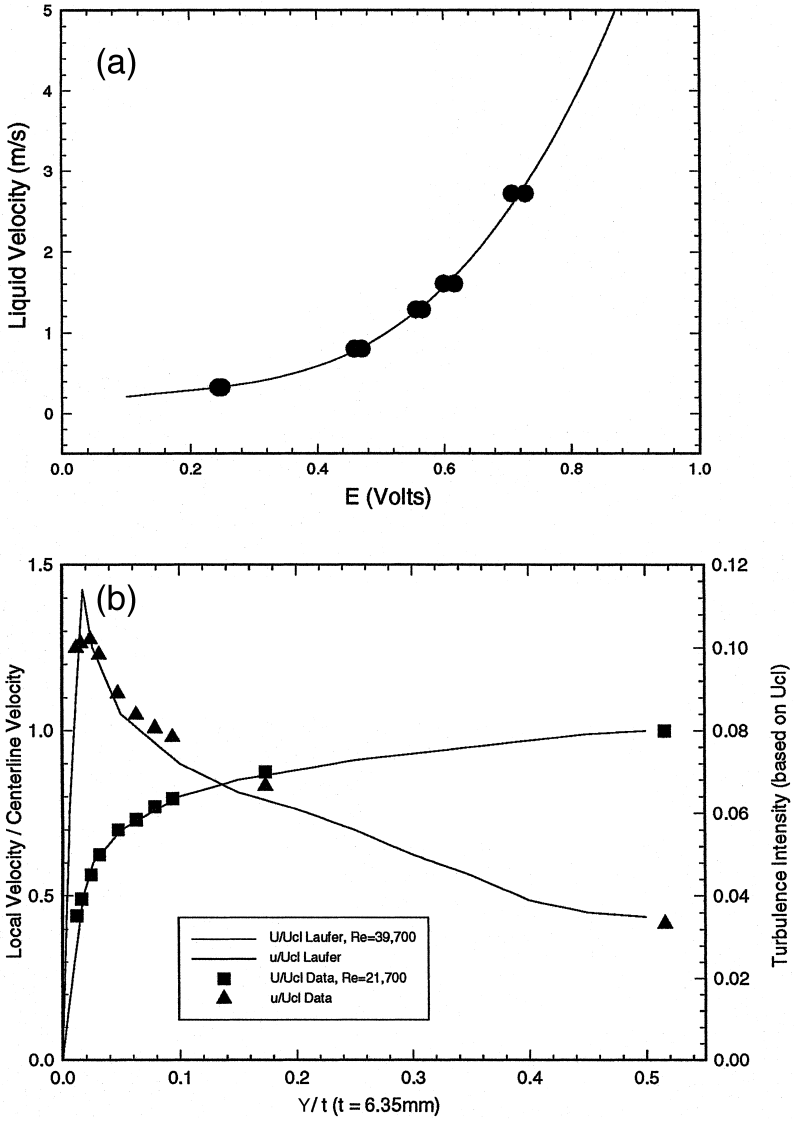

Fig. 3. (a) HFA calibration in single-phase liquid flow; (b) single-phase turbulent profiles compared with Laufer's (1951) data.

the curve were taken before and after the two-phase measurements (presented in Section 3.2) and indicate good repeatability.

Fig. 3(b) shows the mean and fluctuating velocity profiles taken with the HFA probe at $Re = 21{,}700$ along with profiles taken by Laufer (1951) at $Re = 39{,}700$ in a 12.7×152.4 cm duct. The mean profiles agree well; the fluctuating profiles also agree well except that the peak intensity at $Y/t = 0.02$ is somewhat lower than Laufer's. This small disagreement may be explained by the fact that, at a given Reynolds number, the near wall turbulent production is highly sensitive to duct size, with the larger duct sizes having higher turbulence intensities [Laufer (1951)]. In any case, the current data, showing smooth and reasonable turbulent profiles, provides a measure of confidence in using HFA to obtain liquid velocity statistics.

3.2. Two-phase flow

Three annular flow conditions were investigated with the following superficial velocities: case (1) $j_l = 1.3$ m/s, $j_g = 12.8$ m/s; case (2) $j_l = 0.65$ m/s, $j_g = 20.4$ m/s and case (3) $j_l = 0.65$ m/s, $j_g = 25.0$ m/s. These conditions were chosen to cover a broad range of available gas and liquid flow rates while still maintaining a steady (non-chugging) annular flow. The conditions represent quite different flow tropologies: qualitatively, case 1 consists of a lower overall void fraction, with a thicker and more turbulent liquid film on the wall, while cases 2 and 3 have a thinner, steadier film structure. According to the flow pattern map of Hewitt and Roberts (1969), case 1 lies near the border of the annular and churn–turbulent regime while cases 2 and 3 are more completely annular. Table 3 summarizes the conditions, including average void fraction and mean film thickness. The mean film thickness, which provides approximate film depths for each flow condition, was calculated as:

$$h = \frac{(1 - \bar{\alpha})Wt}{2(W + t)}$$

where W is test section width, t is test section thickness, and $\bar{\alpha}$ is average void fraction. Further discussion based on quantitative measurements for each flow condition is given next.

Table 3
Summary of test cases

Case	j_l (m/s)	j_g (m/s)	$\bar{\alpha}_{valves}$	$\bar{\alpha}_{HFA}$	Mean film thickness (mm)
1	1.3	12.8	0.76	0.73	0.69
2	0.65	20.4	0.85	0.83	0.43
3	0.65	25.0	0.88	0.86	0.36

3.3. General flow topology

In Fig. 4, measurements of interfacial velocity and void fraction are presented. The void fraction for all test cases increases rather steeply for $Y/t < 0.1$, increases more gradually for $0.1 < Y/t < 0.2$ and is relatively constant for $0.2 < Y/t < 0.5$. These regions, indicated in

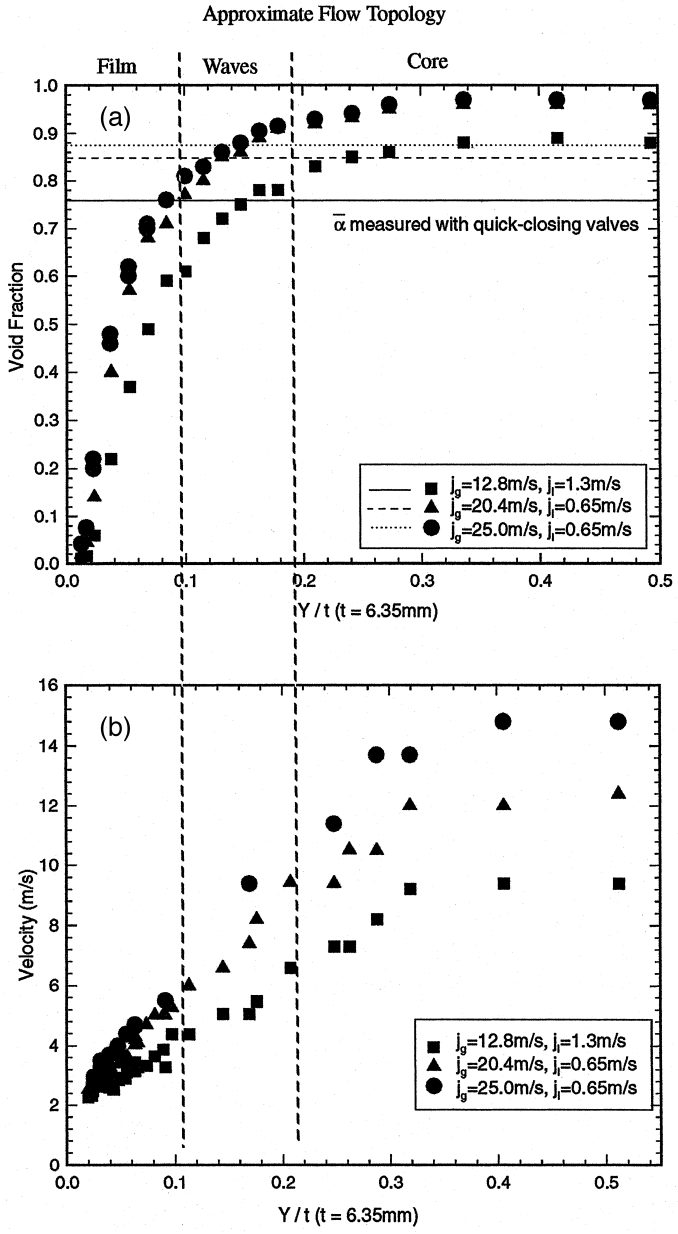

Fig. 4. (a) Local HFA void fraction measurements compared to average measurements; (b) HFA interfacial velocity measured using cross-correlation.

Fig. 4, may be roughly interpreted as the liquid film, interfacial wave, and droplet core regions. The average of the local measurements agreed within 3% of the cross-section averaged void fraction obtained with the quick-closing valves, as shown in Table 3. This provides a measure of confirmation that the HFA processing algorithm is being correctly applied. The random uncertainty in average void fraction ($\pm 2\%$) was estimated by repeating measurements of the same flow conditions with the quick-closing valves. The bias uncertainty is $< 3\%$, based on previous experience with this technique.

3.4. Near wall measurements

In Fig. 5, near wall measurements of liquid velocity, interfacial velocity, liquid turbulence intensity and void fraction are presented. These measurements were taken over several days, using appropriate single-phase calibration performed before and after each data set. There are several sources of uncertainty in the measurements: (a) calibration uncertainty; (b) phase discrimination uncertainty; and (c) statistical uncertainty. To assess the magnitude of (a), calibration curves were generated using maximum uncertainties in each calibration voltage point which led to an uncertainty range in liquid velocity and turbulence intensity. The uncertainties due to (b) and (c) were estimated by examining the scatter in data taken in immediate succession. The final estimate of uncertainty is shown as error bars in Fig. 5. Note that the relative difference in velocity and turbulence intensity between the test cases would, generally, be present. This is because the HFA measurements for the test cases were taken in quick succession at each specified Y location, before moving to the next Y location.

The liquid velocity obtained via calibrated HFA measurements can be compared with the interfacial velocity obtained by cross-correlation in Fig. 5. Most of the data points below $Y/t = 0.06$ agree within $\pm 10\%$. This indicates that, near the wall, the interfaces in the film move at a mean velocity which is close to that of the liquid phase. Beyond $Y/t = 0.05$, the interfacial velocity begins to rise more steeply. This seems to be a logical result as the high velocity gas core must begin to influence the velocity of the liquid waves near the outer region of the film. However, the liquid velocity, especially for cases 2 and 3, do not show this trend. It is likely that the calibration for liquid velocity becomes inaccurate as the void fraction increases beyond a certain point. For cases 2 and 3, near $Y/t = 0.06$, the void fraction exceeds 0.65, and the liquid phase is probably in the form of waves and droplets. These waves and droplets strike the probe and, as a result, may produce biased velocity fields. In addition, the uncertainty in the discrimination technique becomes more problematic as the void fraction, α, increases and will then contribute to the overall uncertainty. For void fractions under 0.5, the liquid field is largely continuous, and the calibration is more accurately applied.

The measured liquid turbulence intensities show a peaking near the wall and a relatively constant profile throughout the rest of the film. These observations are consistent with those of Lorencez et al. (1997) who studied horizontal gas–liquid stratified flow. Their study also showed that the liquid turbulence level increased in the presence of a shearing gas flow. Here, the near wall turbulence level for case 1 is greater than that for cases 2 and 3, and all are higher than for single-phase liquid flow. The measured total pressure gradient is significantly higher for case 1 and, since the mean velocity near the wall is about the same as case 2, would

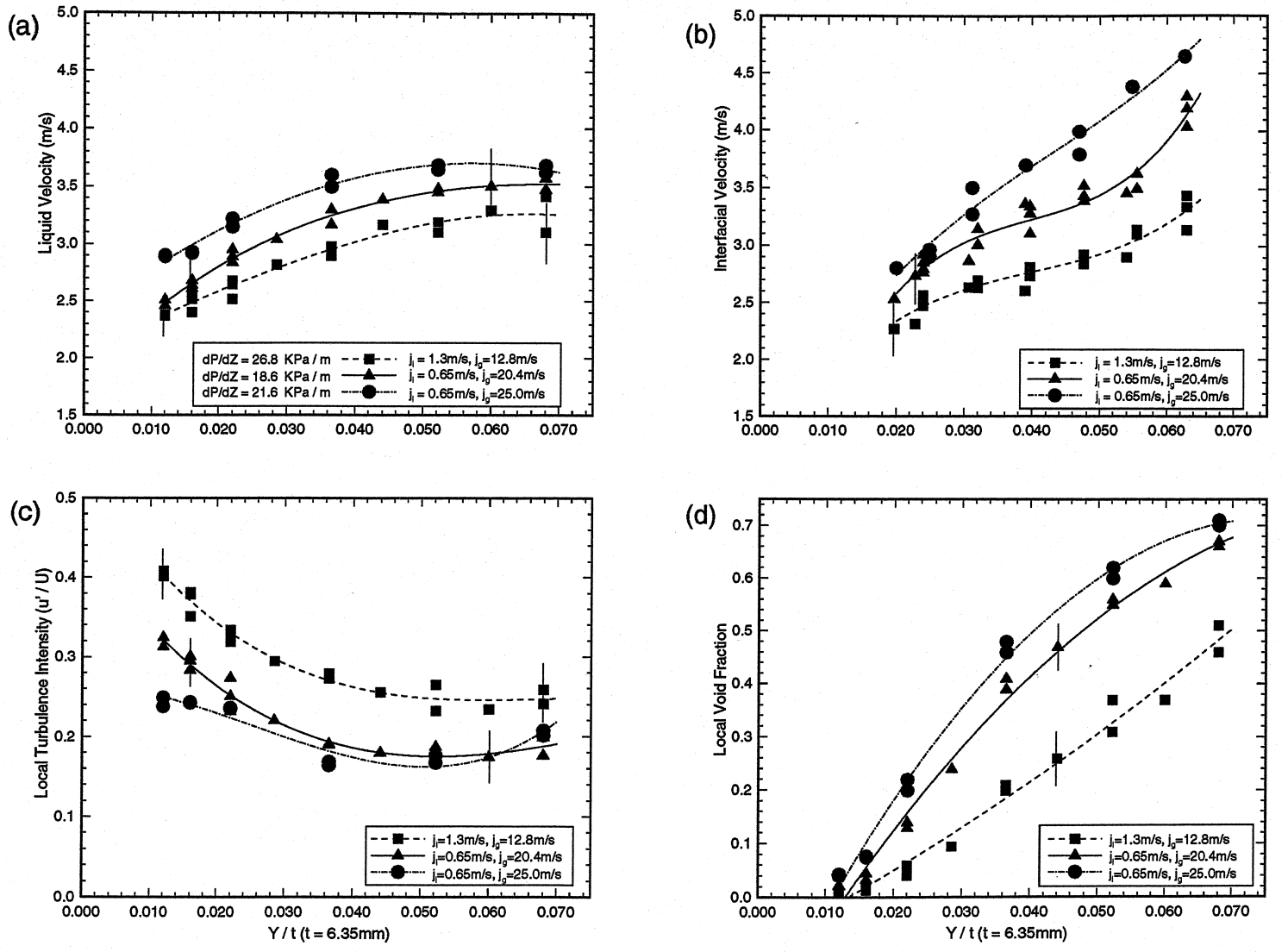

Fig. 5. Near-wall HFA data; (a) liquid velocity using calibration; (b) interfacial velocity using cross-correlation; (c) turbulence intensity; (d) void fraction.

seem to be related to the turbulence level in the film. This relationship is examined in more detail in the following section.

3.5. Law-of-the-wall formulation for wall shear

An expression for wall shear as a function of fluid density, ρ, viscosity, v, velocity and turbulent energy may be derived using single-phase law-of-the-wall for smooth walls as:

$$u^+ = \frac{1}{\kappa}\ln y^+ + C \tag{1}$$

where

$$u^+ = \frac{u}{u_*} \tag{2}$$

u = mean velocity parallel to wall,

$$u_* = \sqrt{\frac{\tau_w}{\rho}} \tag{3}$$

τ_w = average stress at wall,

$$y^+ = \frac{yu_*}{v} \tag{4}$$

y = dimension normal to wall.

$$\text{Defining } \ln C_2 = \kappa C, \tag{5}$$

$$\frac{u}{u_*} = \frac{1}{\kappa}\ln\left(\frac{yu_*C_2}{v}\right) \tag{6}$$

or

$$\rho\frac{u}{\tau_w} = \frac{1}{u_*}\frac{1}{\kappa}\ln\left(\frac{yu_*C_2}{v}\right). \tag{7}$$

To relate local shear stress to turbulent kinetic energy, k, the following assumption is made:

$$\tau_p = \sqrt{C_\mu}\rho k. \tag{8}$$

This is a good assumption in equilibrium boundary layers, with no strong accelerations or decelerations, and where the boundary layer is attached ($C_\mu = 0.09$). Both assumptions imply standard k–ε formulation. The quantity τ_p represents the shear stress at a point in the logarithmic layer ($y^+ \backsim 14$). If $\tau_w \backsim \tau_p$, then Eq. (7) becomes:

$$\tau_w = \frac{\rho u\sqrt{k}}{\frac{1}{\kappa C_\mu^{0.25}}\ln\left(C_2 C_\mu^{0.25}\frac{\sqrt{k}y}{v}\right)} \tag{9}$$

where, for single-phase flow over smooth walls

$$\kappa = 0.4,$$
$$C_2 = 7.39.$$

The data was plotted using wall coordinates in Fig. 6(a). The friction velocity, u_*, was determined from the measured frictional pressure drop, ΔP_f, as:

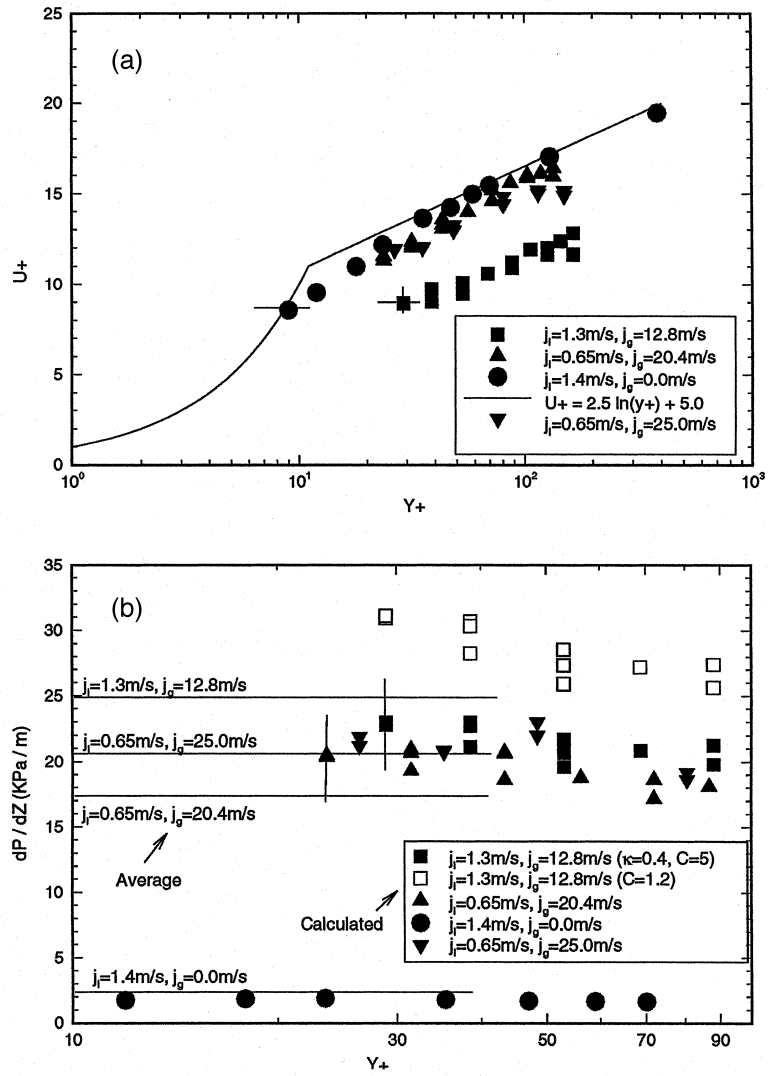

Fig. 6. (a) Liquid phase velocity profiles plotted using inner variables; (b) calculated local frictional dP/dZ from HFA measurements using law-of-wall formulation compared to average dP/dZ measurements.

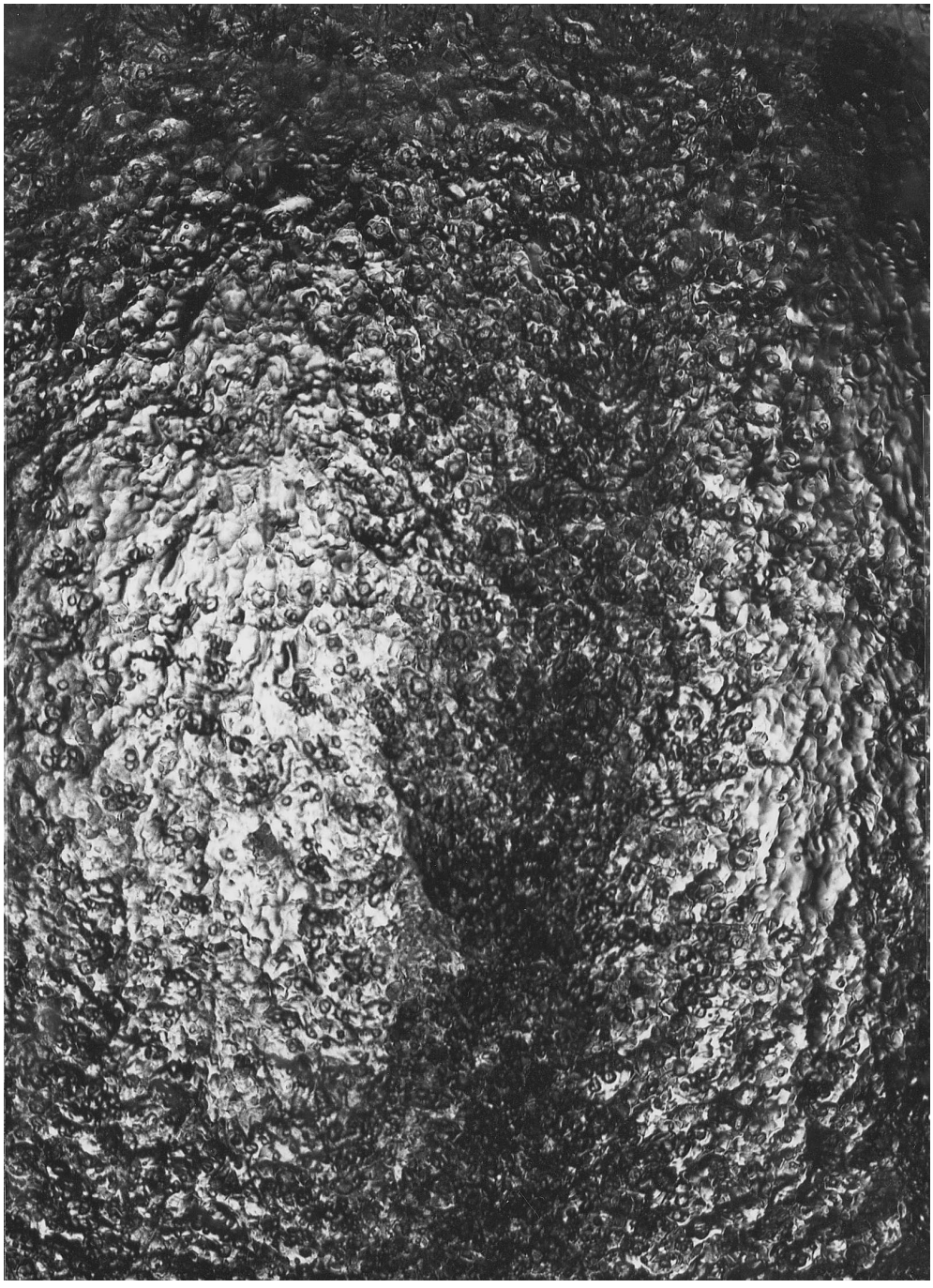

Fig. 7. Photograph of case 1 condition (j_l = 1.3 m/s, j_g = 12.8 m/s). Magnification = 2.5.

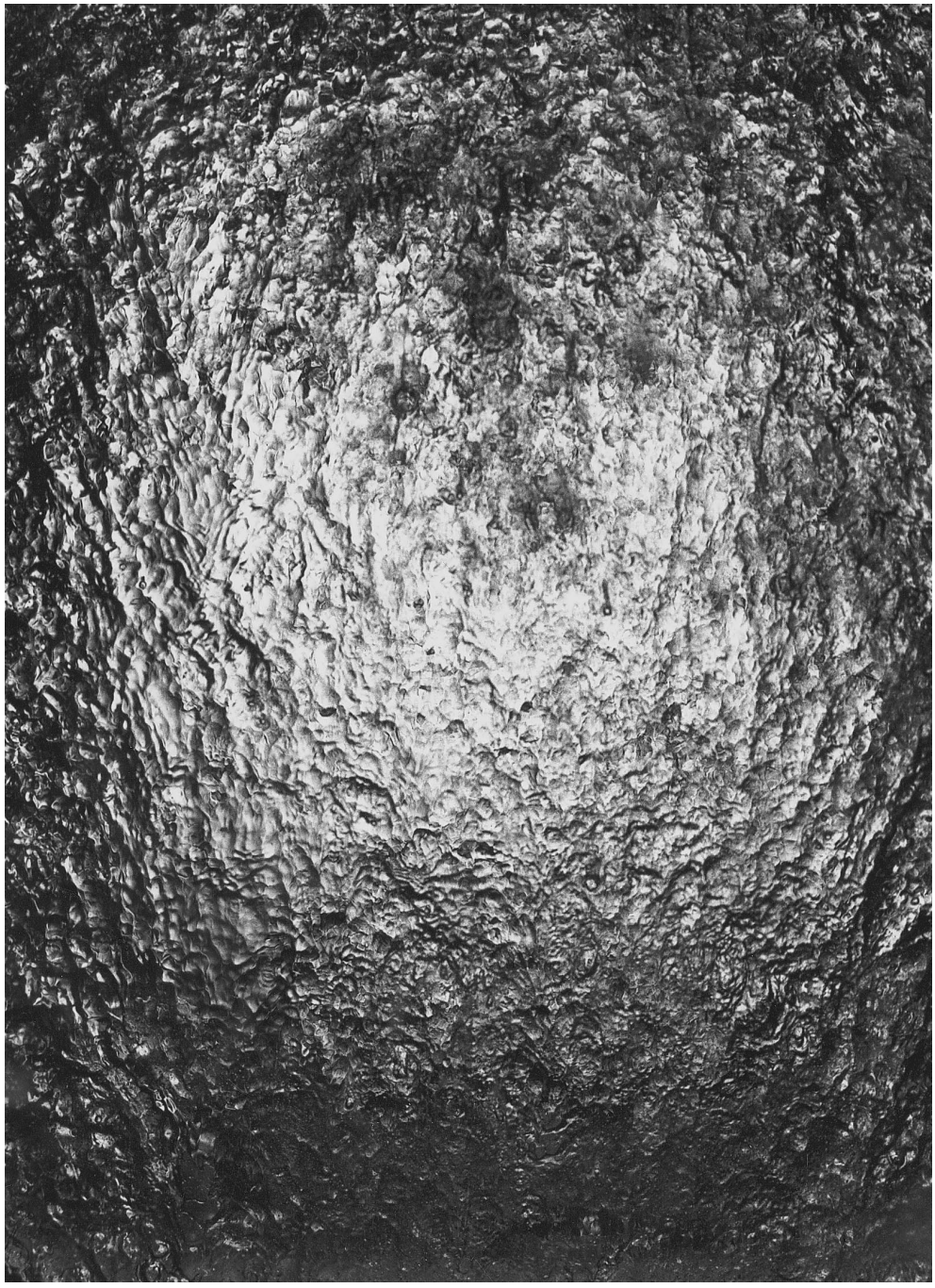

Fig. 8. Photograph of case 2 condition ($j_l = 0.65$ m/s, $j_g = 20.4$ m/s). Magnification = 2.5.

$$u_* = \sqrt{\frac{\tau_w}{\rho}} = \sqrt{\frac{1}{\rho}\frac{\Delta P_f}{4}\frac{D_H}{L}} \tag{10}$$

where L is the axial distance between pressure taps. Previous studies in vertical air–water annular flow in a 25.4 mm diameter tube [Govan et al. (1989)] have shown that the local wall shear measurements are consistent with the average stress obtained with Eq. (10). This provides some confidence in using Eq. (10) as described.

The single-phase liquid profile in Fig. 6(a) is in good agreement with the single-phase wall-bounded flow theory, which includes both the viscous sublayer ($y^+ < 14$) and logarithmic zone ($14 < y^+ < 300$). The liquid phase velocity profile for cases 2 and 3 also agrees reasonably well with the single-phase theory. The liquid phase velocity profile for case 1, however, does not agree with single-phase theory; in particular, the intercept (C) is less. This implies that the film structure is affecting the wall shear and, in fact, is increasing it for a given velocity profile in the film.

Similar trends have been observed in recent studies of wall-bounded bubbly flows. Both Velidandla et al. (1996) and Marie et al. (1997) observed that the slope and intercept of the liquid velocity profile in the logarithmic zone in bubbly flow were lower than in single-phase flow. As noted by Schubauer and Tchen (1961), lowering C implies that the effective roughness, in this case due to the bubbles, is increasing at the surface and that the laminar sub-layer thickness extends closer to the wall. In air–water annular flows, Hewitt et al. (1990) observed that air bubbles were continuously entrained, broken up and released by the rolling action in the liquid film. Because the liquid film in case 1 is thicker than in cases 2 and 3, it is likely that roll waves create more bubbles in case 1, and would therefore help to explain the deviation of the velocity profile from single-phase theory. In Figs. 7 and 8, still photographs reveal that, indeed, more bubbles appeared to be present in the liquid film for case 1 vs case 2.

The near wall turbulence levels for cases 1–3 have already been presented; now, Eqs. (9) and (10) are used to predict the pressure gradient as a function of turbulent kinetic energy, fluid properties, fluid velocity and law-of-the-wall constants. Because u' was the only fluctuating velocity measured, v' and w' had to be estimated in order to obtain k. In most near wall flows, the turbulence is highly anisotropic with u' being much larger than v' or w'. Here, u' was taken as $3v' = 3w'$ which is in line with single phase measurements for $y^+ < 50$ (Laufer, 1951). As will be seen next, this estimate for k yields reasonable comparison between data and theory.

Fig. 6(b) shows the predictions of frictional pressure gradient calculated from the local HFA measurements as well as the direct measurements. The calculated single-phase and cases 2 and 3 results, using law-of-the-wall constants from single-phase theory, agree reasonably well with the direct measurements. On the other hand, the calculated results for case 1, using law-of-the-wall constants from single-phase theory, are lower than expected, based on relative comparisons between the cases. The prediction improves if a modified value of $C = 1.2$ is used in Eq. (9), as derived from a curve fit in Fig. 6(a) for case 1. It therefore appears that Eq. (9) captures the appropriate relationship between turbulence and wall shear in annular flows provided that the proper law-of-the-wall constants are used in the formulation. These constants appear to be equal to the single-phase values in a "clean" annular flow, where the film is thin and where less bubbles are present. If the film is thicker and more turbulent, with bubbles present, the constants, most notably the intercept, C, will decrease. Further experiments over a

wider range of annular flow conditions would be necessary to determine the functional relationship between the law-of-the-wall constants and other pertinent flow parameters.

4. Conclusions

Local measurements of void fraction, liquid mean and fluctuating velocity were acquired in the liquid film in vertical air–water annular flow to examine the relationship between the turbulent structure in the film and the wall shear stress in the context of the classical law-of-the-wall formulation. The measurements showed that, for well defined annular flow, the law-of-the-wall developed in single-phase flow is applicable and may be used to predict the wall shear stress in the usual manner. However, for annular flows near the transition regime, where the film is thicker, more chaotic and where bubbles are being entrained, a modified log-law should be used with a smaller value of the intercept constant. Suggested areas for further work include a broader range of annular flow experiments to better understand the relationship between the flow structure and the law-of-the-wall formulation. In particular, as the wall shear is related to $\sqrt{k}$, the increase in wall shear for particular annular flow conditions may be predicted via a model capturing the increase in kinetic energy for those flows.

Acknowledgements

The author is grateful to S. M. Ettorre for inspiring this work, to R. Kumar for his informative discussions and to C. Zarnofsky for his technical assistance.

References

Asali, J.C., Hanratty, T.J., 1993. Ripples generated on a liquid film at high velocities. Int. J. Multiphase Flow 19, 229–243.

Bellinghausen, R., Renz, U., 1992. Heat transfer and film thickness during condensation of steam flowing at high velocity in a vertical pipe. Int. J. Heat Mass Transfer 35, 683–689.

Govan, A.H., Hewitt, G.F., Owen, D.G., Burnett, G., 1989. Wall shear stress measurements in vertical air–water annular two-phase flow. Int. J. Multiphase Flow 15, 307–325.

Hewitt, G.F., Roberts, D.N., 1969. Studies of two-phase patterns by simultaneous X-ray and flash photography, AERE-M 2159. H.M.S.O.

Hewitt, G.F., Whalley, P.B., 1989. Vertical annular two-phase flow, multiphase science and technology, Chap. 2, 4. Hemisphere Publishing, New York.

Hewitt, G.F., Jayanti, S., Hope, C.B., 1990. Structure of thin liquid films in gas–liquid horizontal flow. Int. J. Multiphase Flow 16, 951–957.

Laufer, J., 1951. Investigation of turbulent flow in a two-dimensional channel. NACA rep. 1053.

Lee, S.J., 1982. The development of a digital data processing system for two-phase turbulence data. Masters thesis, Rensselaer Polytechnic Institute, Troy, N.Y.

Lorencez, C., Nasr-Esfahany, M., Kawaji, M., Ojha, M., 1997. Liquid turbulence structure at a sheared and wavy gas–liquid interface. Int. J. Multiphase Flow 23, 205–226.

Marie, J.L., Moursali, E., Tran-Cong, S., 1997. Similarity law and turbulence intensity profiles in a bubbly boundary layer at low void fractions. Int. J. Multiphase Flow 23, 227–247.

Schubauer, G.B., Tchen, C.M., 1961. Turbulent flow. Princeton Aeronautical Paperbacks. Princeton University Press, Princeton, N.J.

Velidandla, V., Putta, S., Roy, R.P., 1996. Velocity field in isothermal turbulent bubbly gas–liquid flow through a pipe. Exp. in Fluids 21, 347–356.